Universal Entanglement Spectrum in One-Dimensional Gapless Symmetry Protected Topological States

Xue-Jia Yu,[1,2,*] Sheng Yang,[3,*] Hai-Qing Lin,[3] and Shao-Kai Jian[4,†]
[1]Department of Physics, Fuzhou University, Fuzhou 350116, Fujian, China
[2]Fujian Key Laboratory of Quantum Information and Quantum Optics, College of Physics and Information Engineering, Fuzhou University, Fuzhou, Fujian 350108, China
[3]Institute for Advanced Study in Physics and School of Physics, Zhejiang University, Hangzhou 310058, China
[4]Department of Physics and Engineering Physics, Tulane University, New Orleans, Louisiana 70118, USA

(Received 13 February 2024; revised 16 May 2024; accepted 11 June 2024; published 12 July 2024)

Quantum entanglement marks a definitive feature of topological states. However, the entanglement spectrum remains insufficiently explored for topological states without a bulk energy gap. Using a combination of field theory and numerical techniques, we accurately calculate and analyze the entanglement spectrum of gapless symmetry protected topological states in one dimension. We highlight that the universal entanglement spectrum not only encodes the nontrivial edge degeneracy, generalizing the Li-Haldane conjecture to gapless topological states, but also contains the operator content of the underlying boundary conformal field theory. This implies that the bulk wave function can act as a fingerprint of both quantum criticality and topology in gapless symmetry protected topological states. We also identify a symmetry enriched conformal boundary condition that goes beyond the conventional conformal boundary condition.

DOI: 10.1103/PhysRevLett.133.026601

Introduction.—Topological phases are novel many-body states featuring nonlocal order parameters and unusual entanglement properties. It is well understood that the quantum entanglement structure is necessary to describe these topological phases, since they fail to be distinguished by local observables in the bulk. For instance, as noticed in the famous Li-Haldane conjecture [1], the bulk entanglement spectrum encodes the information on the boundary Hamiltonian. More explicitly, this conjecture states that the bulk low-lying entanglement spectrum is in one-to-one correspondence with the universal part of the many-body energy spectrum at the boundary of the system, which indicates that the bulk ground state wave function can capture boundary universal information, such as edge mode degeneracy of the gapped topological phase [2–7].

Symmetry protected topological phases (SPT) [8–12], as one subclass of the topological phases, refers to the topological states that are only nontrivial under certain global symmetry. While the bulk of SPTs is gapped, nontrivial gapless states emerge at the boundary. Despite the crucial role of the bulk gap in defining topological phases, recent research [13–31] has revealed that many key features of topological physics persist in the gapless case, even in the presence of the nontrivial coupling between the topological edge modes and the critical bulk modes. This extension is termed gapless symmetry-protected topological phases (gSPTs) [24–51], This development has led to the discovery of new quantum critical points (QCPs) and phases in $1+1$D with unusual string operators that imply symmetry-protected topological edge modes, classified by conformal boundary conditions [25,26,52].

In the context of gSPTs, the question of how universal the Li-Haldane conjecture remains an interesting open question. We note that these gapless topological states not only host topological protected edge modes, but also have bulk critical fluctuations described by a conformal field theory (CFT) [15,24–31,53–64]. The entanglement spectrum in CFTs has been extensively studied [1,65–77], which shows that it contains universal information that goes beyond the entanglement entropy. With powerful conformal invariance in two dimensions, the entanglement spectrum in a $1+1$D CFT in various geometries can be exactly mapped to the energy spectrum with an open boundary condition [78–81], aligning with the operator content [82] of the underlying boundary CFT [83–85]. Hence, this raises an intriguing question: On one hand, entanglement spectrum reveals the information on nontrivial boundary states for the topological phases according to the Li-Haldane conjecture. On the other hand, it also contains the operator content in a boundary CFT prescribed presumably by the entanglement cut. What is the interplay between these two interesting phenomena in $1+1$D gapless topological states? Can we extract the topology and boundary CFT information solely from the bulk wave function according to entanglement spectrum?

In this Letter, we study different families of quantum spin chains that exhibit different types of gSPTs in one dimension. Each family contains symmetry protected

topological edge modes that are described by the corresponding boundary CFT. By examining their entanglement spectrum and energy spectrum, we show that the bulk entanglement spectrum is in one-to-one correspondence with the energy spectrum at the edge of the system, which means that the entanglement spectrum contains the information of both the topological edge state and the corresponding boundary CFT operator content. Additionally, thanks to conformal symmetry present in the gSPTs, the universal spectrum correspondence can be understood theoretically, thus establishing a solid bulk-boundary correspondence in $1+1$D gSPTs. We also identify a symmetry enriched conformal boundary condition in the free boson CFT beyond the conventional Dirichlet boundary condition.

Entanglement spectrum of gapped SPT.—The entanglement spectrum consists of the eigenvalues of the modular or entanglement Hamiltonian $\tilde{H}_A$, which is related to the reduced density matrix ρ_A of the subsystem A by

$$\rho_A = \mathrm{Tr}_B|\Psi\rangle\langle\Psi| = \sum_\alpha e^{-\ln\lambda_\alpha}|\Psi_\alpha^A\rangle\langle\Psi_\alpha^A| = e^{-\tilde{H}_A}. \quad (1)$$

Here, $|\Psi>$ is the ground state wave function of the Hamiltonian, and λ_α is the eigenvalue of ρ_A. In our study of 1D quantum chain, $A=\{1,2,\ldots L/2\}$ and $B=\{L/2+1,\ldots L\}$ represent a spatial bipartition of the whole chain. The boundary points between A and B (more generally, the boundary between A and B) are called the entangling surface (or entanglement cut).

As a warm-up, we first study the 1D version of Li-Haldane conjecture in the following cluster SPT model [25,86,87], $H=-\sum_{i=1}^{L}\sigma_i^z\sigma_{i+1}^x\sigma_{i+2}^z - h\sum_{i=1}^{L}\sigma_i^x$. The Pauli matrices $\sigma_i^{x/z}$ represent the spin-1/2 degrees of freedom on site i. This model hosts a gapped SPT phase at $h<1$ and a trivial phase at $h>1$ [86]. While the ground state is unique in the trivial phase, the SPT phase features a fourfold degeneracy from two edges in open boundary condition (OBC). Figures 1(a) and 1(c) illustrate the energy spectrum under OBC for the trivial and SPT phases, respectively. The degeneracy arises from zero-energy edge states at either end of the chain. The entanglement spectrum under periodic boundary conditions (PBC) for the trivial and SPT phases are shown in Figs. 1(b) and 1(d), respectively. Remarkably, the "lowest-energy" structure, highlighted by red boxes in Fig. 1, of the entanglement spectrum faithfully reproduces the (non) degeneracy of the (trivial) SPT phase [67,75,88,89].

Entanglement spectrum in symmetry enriched QCPs.—Until now, different families of gSPTs have been identified in the literature [27,28,30,31]: nonintrinsic gSPTs usually emerge at critical points between SPTs and spontaneous symmetry breaking phases and exhibit a partial set of edge modes from the adjacent gapped SPT, referred to as symmetry-enriched QCPs; conversely, intrinsically gSPTs

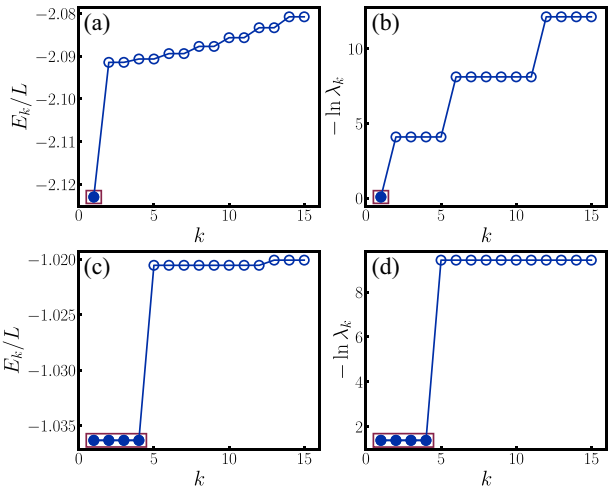

FIG. 1. OBC energy spectrum and PBC bulk entanglement spectrum for (a)–(b) the trivial phase ($h=2.0$) and (c)–(d) the SPT phase ($h=0.5$). The system size is $L=64$ for OBC and $L=128$ for PBC, and k counts the spectrum from the lowest-lying levels. The ground state manifolds of the entanglement spectrum show the same number of levels as the physical ground state manifolds, as indicated by the red boxes.

are usually stable phases without a gapped counterpart. For instance, emergent anomalies in intrinsically gSPTs could not arise in a gapped phase in the same dimension with the same symmetry. In this work, we refer to these phases as gapless symmetry-protected topological states.

As an example of symmetry enriched QCPs, we consider the generalized cluster Ising chain [24,25,90,91],

$$H_{\mathrm{CI}} = -\sum_{i=1}^{L}\sigma_i^z\sigma_{i+1}^x\sigma_{i+2}^z - h\sum_{i=1}^{L}\sigma_i^z\sigma_{i+1}^z. \quad (2)$$

This model possesses a $\mathbb{Z}_2$ spin-flip symmetry and a time-reversal symmetry $\mathbb{Z}_2^T$: $P=\prod_i\sigma_i^x$ and $T=\mathbb{K}$ (complex conjugation). By adjusting the tuning parameter h, the system undergoes a transition between a ferromagnetic (FM) phase and an SPT phase, with the latter sometimes referred to as the cluster SPT phase. The FM-SPT transition is described by a symmetry enriched Ising CFT, where the time-reversal symmetry acts nontrivially on the string operator. In a semi-infinite geometry, the string operator (symmetry flux) $\sigma_1^z\sigma_2^y\prod_{i=3}^{\infty}\sigma_i^x$ has a nontrivial charge under time reversal symmetry, making it distinct from a normal Ising CFT. Moreover, the charged string operator renders a twofold degenerate algebraic splitting edge mode protected by $\mathbb{Z}_2\times\mathbb{Z}_2^T$ symmetry. Intuitively, because σ_1^z commutes with the Hamiltonian in a semi-infinite chain, the edge spontaneously breaks the Ising symmetry. Note that this is not merely a fine-tuned result but protected by the underlying symmetry [24].

To investigate the corresponding bulk-boundary duality, we used the density matrix renormalization group (DMRG)

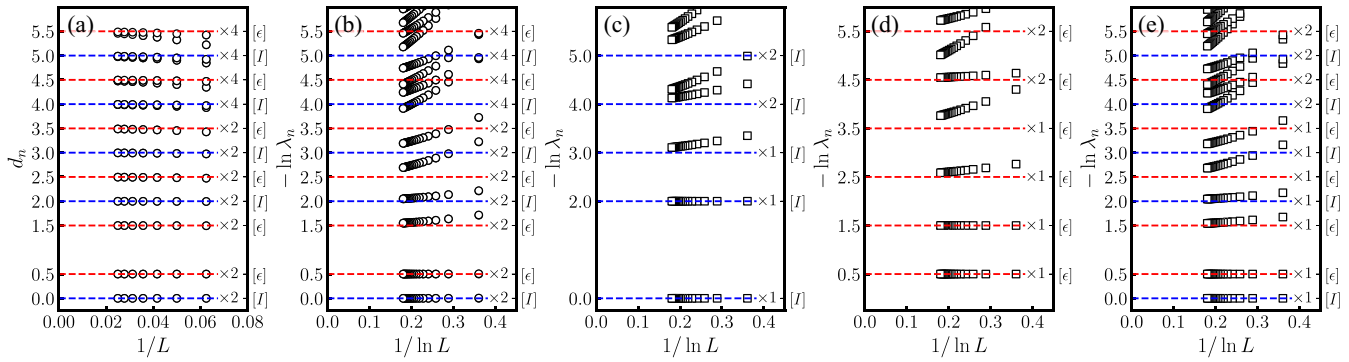

FIG. 2. (a) OBC energy spectrum and (b) PBC entanglement spectrum of the generalized cluster Ising chain Eq. (2) at the QCP $h = 1.0$ for several L. The results of the bulk entanglement spectrum with additional projections on the boundary are shown in (c) for $(1+\sigma_1^z)(1+\sigma_{L/2}^z)$, in (d) for $(1+\sigma_1^z)(1-\sigma_{L/2}^z)$, and in (e) for $(1+\sigma_1^z)$. All the spectra have been rescaled separately such that the first two levels are fixed to the corresponding values. For example, $d_n = 0.5 \times (E_n - E_1)/(E_2 - E_1)$ in (a). Open circles represent a twofold degeneracy while open squares indicate a single degeneracy.

method [92–98] (The details of the algorithm are introduced in the Supplemental Material [99].) to calculate the bulk entanglement spectrum and many-body energy spectrum under OBC, respectively, as shown in Figs. 2(a) and 2(b). After a proper rescaling, we observe that (i) the entanglement spectrum shows the same doubly degeneracy in the OBC energy spectrum, reflecting the nontrivial edge state, (ii) the bulk entanglement spectrum contains the same operator content in the corresponding boundary CFT, and (iii) the algebraic splitting edge mode in our example can be identified through finite-size scaling of the bulk entanglement spectrum (see Sec. VI of the Supplemental Material [99] for a detailed discussion). This example also demonstrates that the bulk wave function nicely encodes the information on the topology and the operator content under OBC. (see Secs. II and III of [99] for discussions on other gSPT families). Furthermore, we verified the stability of the topological degeneracy of the bulk entanglement spectrum under symmetry-preserving local disorders for gSPT phases, to illustrate the generality of our conclusions (see Sec. IV of [99] for details).

Entanglement spectrum in intrinsically gapless SPT phases.—Now, we examine a representative system of the intrinsically gapless SPT phase given by [27]

$$H_{\mathrm{igSPT}} = -\sum_{i=1}^{L}\big(\tau_{2i-1}^z\sigma_{2i}^x\tau_{2i+1}^z + \tau_{2i-1}^y\sigma_{2i}^x\tau_{2i+1}^y + \sigma_{2i}^z\tau_{2i+1}^x\sigma_{2i+2}^z + \Delta\tau_{2i-1}^x\tau_{2i+1}^x\big), \tag{3}$$

where each pair of $(\tau_{2i-1}, \sigma_{2i})$ represents the ith unit cell, and the two species of spins per unit cell are represented by Pauli operators σ^α and τ^α. We focus on $|\Delta| < 1$ for the last term, within which the ground state is an intrinsically gapless SPT state. It is an exactly marginal symmetric perturbation. This Hamiltonian can be obtained by stacking an Ising-ordered Hamiltonian with an XXZ chain through the Kennedy-Tasaki (KT) transformation [27,45]. The low-energy effective theory is described by a $c = 1$ free boson CFT. The system possesses a $\mathbb{Z}_4$ symmetry generated by $U = \prod_i \sigma_{2i}^x e^{i(\pi/4)(1-\tau_{2i-1}^x)}$, which exhibits an emergent anomaly in the low energies. Namely, in the low-energy sector, where $\sigma_{2i-2}^z\sigma_{2i}^z = \tau_{2i-1}^x$, the $\mathbb{Z}_4$ is approximately $U \sim \prod_i \sigma_{2i}^x e^{i(\pi/4)(1-\sigma_{2i-2}^z\sigma_{2i}^z)}$, which is the same anomaly on the boundary of a $2+1$D Levin-Gu SPT phase [106]. This anomaly prevents the system from realizing a unique symmetry-preserving gapped phase. Moreover, in an open chain with a length L, the square of the low-energy symmetry operator fractionalizes onto each end of the boundary [30,31], $U^2 \sim \tau_1^x\sigma_2^z\sigma_{2L}^z$. This charge locally anticommutes with the U symmetry, protecting a twofold ground-state degeneracy.

It is obvious to note that the sublattice magnetization $m_x = \frac{1}{2}\sum_i\langle\tau_{2i-1}^x\rangle$ is a good quantum number for any Δ. Consequently, we can categorize the full spectrum into different sectors labeled by m_x. The results of energy and entanglement spectrum for $\Delta = 0$ are depicted in Figs. 3(a) and 3(b), respectively. We observe that the bulk entanglement spectrum not only exhibits the same degeneracy as the OBC energy spectrum but also shares the same operator content. Both OBC energy spectrum and bulk entanglement spectrum correspond to the operator content of the free boson boundary CFT [78], which suggests that both topological and boundary CFT information can be obtained in the stable critical phase through entanglement spectrum from a bulk wave function.

Entanglement spectrum and boundary CFT.—There exists an immediate relation between the entanglement Hamiltonian and the Hamiltonian of an open boundary chain [79,80]. In the continuum limit, the entanglement cut is modeled by a small spatial region of thickness ϵ at the boundary of A and B. We consider in our examples the ground state of a one-dimensional periodic chain of a

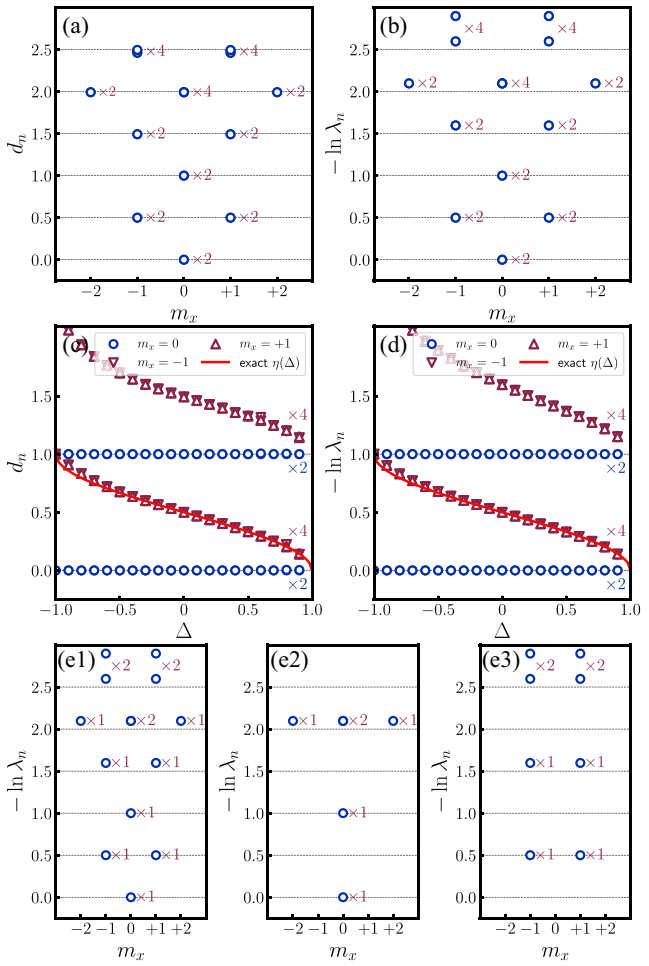

FIG. 3. (a) OBC energy spectrum and (b) PBC entanglement spectrum labeled by the quantum number m_x for the intrinsically gSPT at $\Delta = 0$. The spectra are rescaled separately such that the first two levels within the $m_x = 0$ sector are fixed to 0 and 1, respectively. (c)–(d) The rescaled spectrum within the $m_x = 0$ and ± 1 sectors as a function of Δ. The rescaled value of the first level in the $m_x = \pm 1$ sector is related to the Luttinger parameter and is compared with the exact solution, $\eta(\Delta) = 1 - \arccos(-\Delta)/\pi$ (red solid line). (e1)–(e3) Display the resulting entanglement spectrum for $\Delta = 0$ after the projection $(1 + \sigma^z_{2L})$, $(1 + \sigma^z_L)(1 + \sigma^z_{2L})$, and $(1 - \sigma^z_L)(1 + \sigma^z_{2L})$ from left to right. (e1)–(e3) Are separately rescaled to be directly compared with (b). The simulated system size is $L = 24$ for OBC and $L = 64$ for PBC; the colored numbers indicate the degeneracy of each level.

length L with a bipartition $A : (-L/4, L/4)$ and the complement B as shown in Fig. 4(a). Notice that we shift the entanglement cut from $(0, L/2)$ to $(-L/4, L/4)$ for simplicity without loss of generality. The manifold of the Euclidean path integral is given by an infinite cylinder with two entanglement cuts with a radius ϵ, as shown in Fig. 4(b). The infinite length of the cylinder presents a projection to the ground state in Euclidean path integral. A complex number $z = z + L$ labels the cylinder with the imaginary time in the direction of $\mathrm{Im}(z)$, and the

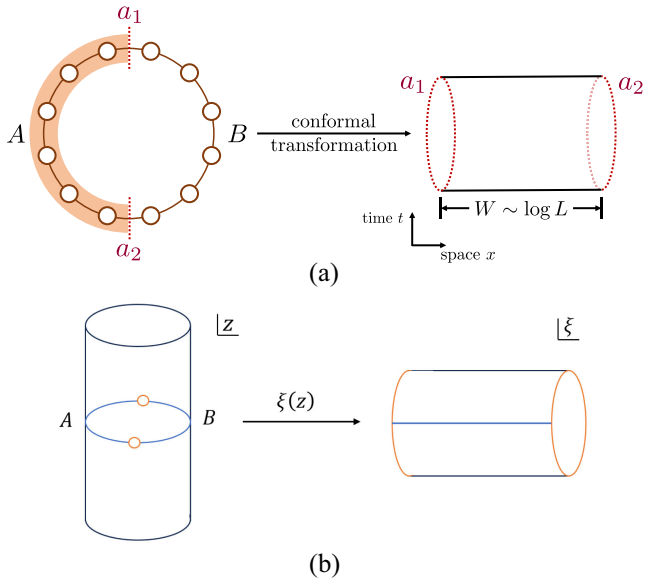

FIG. 4. (a) The setup involves a bipartition of one-dimensional periodic spin models. The orange shaded region denotes the subsystem A, and B represents its complement. The red dotted line represents the entanglement cut, and $a_{1,2}$ labels the boundary condition. After conformal transformation, the reduced density matrix maps to a cylinder (annulus) with width $W \sim \log L$. (b) The Euclidean theory is defined in an infinite cylinder with two entanglement cuts with separating subsystems A and B. Via a conformal transformation $\xi(z)$ in Eq. (4), the infinite cylinder with two cuts is mapped to an annulus.

entanglement cut at $z = \pm L/4$. This manifold can be mapped onto an annulus that terminates at the entanglement cuts by

$$\xi(z) = \log\left(\frac{e^{i2\pi z/L} - e^{-i\pi/2}}{e^{i\pi/2} - e^{i2\pi z/L}}\right), \tag{4}$$

where $\xi = \xi + 2\pi i$ represents the coordinate of the annulus in Fig. 4(b) with $\xi = x + it$. The two boundaries of the annulus are the conformal image of two entanglement cuts at $\xi \approx \pm \log(2L/\pi\epsilon)$, which leads to the width of the annulus

$$W = 2\log\frac{2L}{\pi\epsilon}. \tag{5}$$

After this conformal transformation, the entanglement Hamiltonian is then the conformal image that generates the translation in the $\mathrm{Im}(\xi)$ direction. Hence, the entanglement spectrum is equivalent to the energy spectrum in the annulus with the boundary conditions given at the entanglement cuts. When the "low-energy" part of the spectrum is concerned, these boundary conditions will flow to conformal boundary condition, which we labeled by a_1 and a_2. Given the conformal boundary conditions, a_1 and a_2, and the annulus width W, the entanglement spectrum reads

$$E_j^{(a_1,a_2)} = \frac{\pi}{W}\left(-\frac{c}{24} + \Delta_j^{(a_1,a_2)}\right), \tag{6}$$

where $\Delta_j^{(a_1,a_2)}$ is the scaling dimension of the allowed operators consistent with the conformal boundary conditions a_1 and a_2, and c is the central charge of the underlying CFT. Notice that the energy level is inversely proportional to the annulus width, W, and via the conformal transformation, the entanglement spectrum is, on the other hand, inversely proportional to $\log L$ in Eq. (5) (see Sec. V of [99] for a detailed discussion).

A bipartition of Hilbert space is subtle for a quantum field theory [80,107]. This subtlety can be resolved by considering a finite lattice system and then taking the thermodynamic limit by sending the number of sites to infinite. With the lattice regularization, different conditions on the entanglement cut can be applied. For instance, the "clear cut" refers to a bipartition of two Hilbert spaces naturally defined by $\mathcal{H}_A = \otimes_{i\in A}\mathcal{H}_i$, $\mathcal{H}_B = \otimes_{i\in B}\mathcal{H}_i$ on a lattice system, with $\mathcal{H}_i$ the local Hilbert space at the ith site. Also, a projection of the wave function onto a complete set of commuting operators at the entanglement cut is another way to make the bipartition well defined in field theory. This corresponds to projections on the adjacent site of the entanglement cut in the lattice regularization.

In the symmetry enriched Ising QCPs of Eq. (2), the boundary CFT is characterized by a "superposition," $\tilde{\mathbb{I}} \oplus \tilde{\epsilon}$, where $\tilde{\mathbb{I}}$, $\tilde{\epsilon}$ denotes two fixed boundary conditions in the language of boundary CFT [24]. Physically, these two states correspond to the boundary spin pointing towards two opposite directions, and the superposition means the boundary has a spontaneous magnetization as two opposite magnetizations are equivalent. This leads to the operator content $(\tilde{\mathbb{I}} \oplus \tilde{\epsilon}) \times (\tilde{\mathbb{I}} \oplus \tilde{\epsilon}) = 2 \times ([\mathbb{I}] \oplus [\epsilon])$ as seen in Fig. 2. Here, $[\mathbb{I}], [\epsilon], [\sigma]$ label the operator content of the three primary fields in the Ising CFT [57]. It is in sharp contrast to normal Ising CFT whose boundary state is normally $\tilde{\sigma}$, i.e., a free boundary condition without double degeneracy. The boundary condition beyond the clear-cut at the entanglement cut provides an additional knob to control the entanglement spectrum. We introduce the projection operators at the entanglement cut, $P_{L,R} \propto (1 \pm \sigma^z_{1,L/2})$, and investigate the entanglement spectrum of renormalized $P_{L,R}|\psi\rangle$. The effect of the projection is to fix the boundary condition to be $\tilde{\mathbb{I}}$ or $\tilde{\epsilon}$. As a result, we can modify the entanglement spectrum according to $\tilde{\mathbb{I}} \times \tilde{\mathbb{I}} = [\mathbb{I}]$, $\tilde{\mathbb{I}} \times \tilde{\epsilon} = [\epsilon]$ and $\tilde{\mathbb{I}} \times (\tilde{\mathbb{I}} \oplus \tilde{\epsilon}) = [\mathbb{I}] \oplus [\epsilon]$ as shown in Figs. 2(c)–2(f).

Symmetry enriched boundary condition.—In the intrinsically gSPT phases of Eq. (3), which is described by a free boson $c = 1$ CFT, the boundary condition in an open chain goes beyond the conventional Dirichlet boundary condition [28,108]. Recall the Dirichlet boundary condition in a free boson CFT contains states with energy

$$E_{m_x,n} \sim \frac{1}{W}\left(\eta(\Delta) m_x^2 + n\right), \tag{7}$$

where m_x (n) is an integer labeling the topological sector (the descendant state) and $\eta(\Delta) = 1 - \arccos(-\Delta)/\pi$. Here, on the other hand, the boundary state is enriched by the symmetry fractionalization $U^2 = \tau^x_1 \sigma^z_2 \sigma^z_{2L}$ at both edges, namely, on top of a Dirichlet boundary state, an extra label of the spontaneous magnetization $\sigma_{1,2}$ on each edge needs to be specified. Hence, the state is enriched, $|m_x, n, \sigma_1, \sigma_2\rangle$. The boundary condition cannot be obtained by a superposition of conventional boundary conditions in free boson boundary CFT. With a parity symmetry in Eq. (3), those states are classified by distinct parity: $|2k, n, \sigma, \sigma\rangle$ and $|2k+1, n, \sigma, -\sigma\rangle$ (see Sec. VII of [99]), each features a double degeneracy $\sigma = \pm 1$. This explains the double degeneracy of entanglement spectrum as seen in Fig. 3 in the language of boundary CFT. We can also modify the entanglement cut by a projection, i.e., $(1 \pm \sigma^z_L)$ or $(1 \pm \sigma^z_{2L})$. A single projection $(1 + \sigma^z_{2L})$ lifts the double degeneracy and results in the remained states: $|2k, n, 1, 1\rangle$ and $|2k-1, n, 1, -1\rangle$; while a joint projection $(1 + \sigma^z_L) \times (1 + \sigma^z_{2L})$ $[(1 - \sigma^z_L)(1 + \sigma^z_{2L})]$ allows states only with $m_x \in 2\mathbb{Z}$ ($m_x \in 2\mathbb{Z} + 1$), as shown in Figs. 3(e1)–3(e3).

Concluding remarks.—To summarize, we have investigated several families of $1 + 1$D quantum chains featuring gSPTs. Our primary focus has been to establish a one-to-one correspondence between the bulk entanglement spectrum and the edge energy spectrum, both of which align with the topological degeneracy of the topological state and operator content of the underlying boundary CFT. Our finding highlights the universal entanglement spectrum, and thus, opens a new avenue toward understanding of gapless topological phases of matter.

Generalizing our study to higher-dimensional gSPTs poses a significant challenge, as it necessitates an understanding of conformal defects within conformal field theories, which remains a nascent field in higher dimensions. We notice that the construction of two-dimensional gSPTs can be done through decorated domain walls and charges of the symmetry defects [15,24]. Additionally, gapless topological phases in free fermion systems at one or higher dimensions [33,51] are more accessible in numerical simulations of bulk entanglement spectrum. It would be an interesting future direction to systematically investigate the entanglement spectrum in these models and make a connection to the Li-Haldane conjecture.

From the perspective of experimental realization, while directly probing the entanglement spectrum is challenging, instead, a reasonable ansatz of entanglement Hamiltonian can be put forward by leveraging the Bisognao-Wihmann theorem [109] to lattice systems, and subsequently obtained efficiently in the state-of-the-art digital quantum platform via entanglement Hamiltonian learning or analog quantum simulator via quantum variational learning [110–113]

(see Sec. VIII of [99] for a review and discussion). It will be interesting to extend these techniques to explore the entanglement Hamiltonian in gapless SPT states in the future.

Regarding the experimental realization in condensed matter systems, we notice that the Haldane phase has been realized experimentally in 1D quantum spin chains [114]. It is possible to realize the symmetry enriched quantum critical point at the transition between this SPT phase and a spontaneous symmetry breaking phase. Moreover, in two dimensions, the deconfined quantum phase transition between the quantum spin Hall insulator and the s-wave superconducting phase features an intrinsically gSPT [114–116]. Notably, this deconfined phase transition could be experimentally realized in WTe_2 [117]. Finally, in a broader sense, the weakly interacting topological semimetal that features gapless boundary states, such as 3D Weyl semimetal with surface Fermi arc [118–121], can be regarded as a gapless SPT phase. This opens up a promising avenue for realizing gSPT in condensed matter experiments, in which the spectrum could be studied.

We thank Yijian Zou, Fei Yan, Linhao Li, Yunqing Zheng, and Da-Chuan Lu for helpful discussions. Numerical simulations were carried out with the ITENSOR package [122] on the Kirin No. 2 High Performance Cluster supported by the Institute for Fusion Theory and Simulation (IFTS) at Zhejiang University. X.-J. Y. thanks Long Zhang, Limei Xu, Rui-Zhen Huang, Chengxiang Ding, and Hong-Hao Song for collaboration on related projects. X.-J. Y. is supported by a start-up grant XRC-23102 of Fuzhou University. This work is also supported by MOST 2022YFA1402701. The work of S.-K. J. is supported by a start-up grant and a COR Research Fellowship from Tulane University.

Appendix: Symmetry-enriched boundary conditions in the intrinsically gSPT phase.—We provide additional results for the igSPT phase in Eq. (3). Recall that the igSPT model before the KT transformation [27] is a classical Ising chain stacked with an XXZ chain,

$$H_{\mathrm{XXZ}} = -\sum_i \left(\tau^y_{2i-1}\tau^y_{2i+1} + \tau^z_{2i-1}\tau^z_{2i+1} + \Delta\tau^x_{2i-1}\tau^x_{2i+1}\right). \tag{A1}$$

It is well known that the XXZ model is exactly solvable and in the bosonization language, it is described by a free compacted boson with the Lagrangian density

$$\mathcal{L} = \frac{1}{2}\left(\frac{1}{v_F}(\partial_\tau\phi)^2 + v_F(\partial_x\phi)^2\right), \tag{A2}$$

where ϕ denotes the boson field. The spin operators are expressed by $\frac{1}{2}\tau^x_i \approx -(1/2\pi R)\partial_x\phi + A(-1)^i\sin(\phi/R)$, $\frac{1}{2}\tau^y_i \approx \cos(2\pi R\theta)[C + B(-1)^i\cos(\phi/R)]$, and $\frac{1}{2}\tau^z_i \approx \sin(2\pi R\theta)[C + B(-1)^i\cos(\phi/R)]$, where ϕ (θ) denotes the free (dual) boson and A, B, C are nonuniversal constants. The radius R of the bosonic field is determined by the anisotropy parameter Δ via $R = \sqrt{(1/2\pi) - (1/2\pi^2)\arccos(-\Delta)}$.

The boundary condition of the XXZ model with an open boundary corresponds to the Dirichlet boundary condition of the field ϕ, giving rise to the partition function [108]

$$\begin{aligned} Z_{\mathrm{XXZ}} &= \mathrm{Tr}[e^{-\beta H_{\mathrm{XXZ}}}] = \frac{1}{\eta(q)}\sum_{m_x\in\mathbb{Z}} q^{2\pi R^2 m_x^2} \\ &= \sum_{m_x\in\mathbb{Z}}\sum_{n=0}^{\infty} p(n) q^{2\pi R^2 m_x^2 + n}, \end{aligned} \tag{A3}$$

where $q = e^{-\beta\pi v_F/L}$ and $\eta(q) = q^{1/24}\prod_{n=1}^{\infty}(1-q^n)$ is the Dedekind η function. $p(n)$ is the number of partitions of the integer n, e.g., $p(0) = 1, p(1) = 1, p(2) = 2, p(3) = 3, p(4) = 5, \ldots$. From the partition function, the operator content is classified into different topological sectors given by an integer m_x, and within each sector, another integer n denotes the excited state. Hence, in the XXZ sector, the eigenstate $|m_x, n\rangle$ is labeled by two integers m_x and n with the eigenenergy

$$E_{m_x,n} = \frac{\pi v_F}{L}\left(2\pi R^2 m_x^2 + n\right), \tag{A4}$$

and the degeneracy $p(n)$. The topological number m_x is associated with the total spin magnetization $m_x = \sum_i \frac{1}{2}\langle\tau^x_{2i-1}\rangle$, which is a good quantum number in the XXZ model. We consider the number of sites to be even, so m_x is an integer. Before the KT transformation because the XXZ model and the Ising ferromagnet are decoupled, there will be a trivial doubling for all states merely due to the two possible magnetizations.

Because the KT transformation is unitary with an open boundary condition, one expects that its OBC energy spectrum contains the operator content of a free boson CFT with a double degeneracy. However, this degeneracy is nontrivial because now the σ spins and the τ spins are strongly coupled in Eq. (3). Moreover, this double degeneracy cannot be accounted in the conventional boundary states given by two integers m_x and n without the degeneracy. For clarity, we consider a chain with $2L+1$ sites labeled by $i = 0, \ldots, 2L$, where the σ (τ) spin is located at even (odd) site. The model has an open boundary condition that terminates on the σ spins at the site 0 and the site $2L$,

$$\begin{aligned} H_{\mathrm{igSPT}} = -\sigma^z_0\tau^x_1\sigma^z_2 - \sum_{i=1}^{L-1}\big(&\tau^z_{2i-1}\sigma^x_{2i}\tau^z_{2i+1} + \tau^y_{2i-1}\sigma^x_{2i}\tau^y_{2i+1} \\ &+ \sigma^z_{2i}\tau^x_{2i+1}\sigma^z_{2i+2} + \Delta\tau^x_{2i-1}\tau^x_{2i+1}\big). \end{aligned} \tag{A5}$$

We also consider L to be an even number, $L\in 2\mathbb{Z}$. The model respects a parity symmetry,

$$I:\ \tau^{\alpha}_{2i-1} \to \tau^{\alpha}_{2L-(2i-1)}, \qquad \sigma^{\alpha}_{2i} \to \sigma^{\alpha}_{2L-2i}. \tag{A6}$$

Because L is an even integer, the middle site $i = L$ is the σ spin, the parity is a site (bond) parity for the σ (τ) spin. The presence of bond parity symmetry classifies the eigenstate into even and odd parity sectors. The parity is closely related to the topological sector m_x [108], $I = (-1)^{m_x}$.

There is an easy way to see such a degeneracy in the model Eq. (A5). The boundary σ spins, σ^z_0 and σ^z_{2L}, commute with the Hamiltonian Eq. (A5). These two boundary spins are related via the parity transformation. Therefore, the eigenstates can be labeled by $|m_x, n, \sigma_0, \sigma_{2L}\rangle$, which is further classified into two sectors, i.e., even parity: $|m_x = 2k, n, \sigma, \sigma\rangle$ and, odd parity, $|m_x = 2k+1, n, \sigma, \bar{\sigma}\rangle$. Here $\sigma = -\bar{\sigma} = \pm 1$. The boundary spins σ^z_0 and σ^z_{2L} anticommute with the $\mathbb{Z}_4$ symmetry introduced in [27], $U = \prod_i \sigma^x_{2i} e^{i(\pi/4)(1-\tau^x_{2i+1})}$, so every eigenstate is twofold degenerate. Namely, $|m_x = 2k, n, \sigma, \sigma\rangle$ and $|m_x = 2k+1, n, \sigma, \bar{\sigma}\rangle$ are both two-fold degenerate for $\sigma = \pm 1$. In summary, in the presence of inversion symmetry, the spectrum of an open chain given by (A5) can be classified into even and odd parity with energy $E_{m_x=2k,n}$ and $E_{m_x=2k+1,n}$, respectively, and all levels are doubly degenerate. It is worth pointing out that the degeneracy is a consequence of the gapless edge state protected by the $\mathbb{Z}_4$ symmetry, irrespective of the parity symmetry. The presence of the parity symmetry relates the degenerate state with $\sigma_0 = \sigma_{2L}$ ($\sigma_0 = -\sigma_{2L}$) to topological sector $m_x = 2k$ ($m_x = 2k+1$).

To verify this theoretical understanding, we implement projections of the boundary spin $(1 \pm \sigma^z_0)$ and $(1 \pm \sigma^z_{2L})$. For a single projection on one edge, $1 + \sigma^z_0$, the degeneracy is lifted, because only a single nondegenerate edge state is allowed. The parity sector is determined solely by the degree of freedom on the other edge, σ^z_{2L}. A joint projection on both edges, $(1 + \sigma^z_0)(1 + \sigma^z_{2L})$, selects even parity states, $m_x \in 2\mathbb{Z}$. While the other one, $(1 + \sigma^z_0)(1 - \sigma^z_{2L})$, selects odd parity states, $m_x \in 2\mathbb{Z} + 1$. The results of the operator content for this OBC energy spectrum can be seen in Fig. 7 in Supplemental Material Sec. VII [99], where we have performed a direct simulation of Eq. (A5) with boundary projections applied on the energy spectrum to achieve the parity selection described here.

The conformal transformation relates the entanglement spectrum to the operator content in boundary CFT. In particular, the boundary condition a_1 and a_2 also get mapped between two theories. In the current context, it means projection on the boundary σ spins. Hence, the same parity selection exhibits in Fig. 3(e). There, with a periodic boundary condition, σ (τ) spin is defined at even sites $i = 2, 4, \ldots, 2L$ (odd sites $i = 1, 3, \ldots, 2L-1$). We also set L to be an even number $L \in 2\mathbb{Z}$. Then the corresponding projections are acted on σ_L and σ_{2L}, with the specific form

$$P = (1 \pm \sigma^z_L)(1 \pm \sigma^z_{2L}). \tag{A7}$$

As found in Fig. 3(e) that a single projection on σ_L or σ_{2L} can remove the double degeneracy, but the resulting spectrum can still reflect the same operator content of the boundary CFT. Moreover, when the projections on σ_L and σ_{2L} are simultaneously applied, depending on the spin orientations chosen for sites L and $2L$, the contribution from odd or even quantum sectors can be further projected out from the degeneracy-removed entanglement spectrum. The results reveal how implementations of the entanglement cut can affect the bulk entanglement spectrum, consistent with the analysis of operator content of the related boundary CFT.

*These authors contributed equally to this work.
†Contact author: sjian@tulane.edu

[1] H. Li and F. D. M. Haldane, Phys. Rev. Lett. **101**, 010504 (2008).
[2] A. Chandran, M. Hermanns, N. Regnault, and B. A. Bernevig, Phys. Rev. B **84**, 205136 (2011).
[3] Z. Yan and Z. Y. Meng, Nat. Commun. **14**, 2360 (2023).
[4] Z. Liu, R.-Z. Huang, Z. Yan, and D.-X. Yao, Phys. Rev. B **109**, 094416 (2024).
[5] M. Song, J. Zhao, Z. Yan, and Z. Y. Meng, Phys. Rev. B **108**, 075114 (2023).
[6] C. Li, R.-Z. Huang, Y.-M. Ding, Z. Y. Meng, Y.-C. Wang, and Z. Yan, Phys. Rev. B **109**, 195169 (2024).
[7] W. Chen, K. Hida, and B. C. Sanctuary, Phys. Rev. B **67**, 104401 (2003).
[8] X.-G. Wen, Rev. Mod. Phys. **89**, 041004 (2017).
[9] X.-G. Wen, Science **363**, eaal3099 (2019).
[10] Z.-C. Gu and X.-G. Wen, Phys. Rev. B **80**, 155131 (2009).
[11] X. Chen, Z.-C. Gu, Z.-X. Liu, and X.-G. Wen, Science **338**, 1604 (2012).
[12] X.-J. Yu, S.-H. Shi, L. Xu, and Z.-X. Li, Phys. Rev. Lett. **132**, 036704 (2024).
[13] A. Keselman and E. Berg, Phys. Rev. B **91**, 235309 (2015).
[14] M. Cheng and H.-H. Tu, Phys. Rev. B **84**, 094503 (2011).
[15] T. Scaffidi, D. E. Parker, and R. Vasseur, Phys. Rev. X **7**, 041048 (2017).
[16] L. Fidkowski, R. M. Lutchyn, C. Nayak, and M. P. A. Fisher, Phys. Rev. B **84**, 195436 (2011).
[17] J. P. Kestner, B. Wang, J. D. Sau, and S. Das Sarma, Phys. Rev. B **83**, 174409 (2011).
[18] F. Iemini, L. Mazza, D. Rossini, R. Fazio, and S. Diehl, Phys. Rev. Lett. **115**, 156402 (2015).
[19] N. Lang and H. P. Büchler, Phys. Rev. B **92**, 041118(R) (2015).
[20] J. Ruhman and E. Altman, Phys. Rev. B **96**, 085133 (2017).
[21] H.-C. Jiang, Z.-X. Li, A. Seidel, and D.-H. Lee, Sci. Bull. **63**, 753 (2018).
[22] A. Keselman, E. Berg, and P. Azaria, Phys. Rev. B **98**, 214501 (2018).
[23] X.-J. Yu, C. Ding, and L. Xu, Phys. Rev. E **107**, 054122 (2023).

[24] R. Verresen, R. Thorngren, N. G. Jones, and F. Pollmann, Phys. Rev. X **11**, 041059 (2021).
[25] X.-J. Yu, R.-Z. Huang, H.-H. Song, L. Xu, C. Ding, and L. Zhang, Phys. Rev. Lett. **129**, 210601 (2022).
[26] D. E. Parker, T. Scaffidi, and R. Vasseur, Phys. Rev. B **97**, 165114 (2018).
[27] L. Li, M. Oshikawa, and Y. Zheng, arXiv:2307.04788.
[28] L. Li, M. Oshikawa, and Y. Zheng, arXiv:2204.03131.
[29] S.-J. Huang and M. Cheng, arXiv:2310.16878.
[30] R. Wen and A. C. Potter, Phys. Rev. B **107**, 245127 (2023).
[31] R. Wen and A. C. Potter, arXiv:2311.00050.
[32] R. Verresen, N. G. Jones, and F. Pollmann, Phys. Rev. Lett. **120**, 057001 (2018).
[33] R. Verresen, arXiv:2003.05453.
[34] S. Liu, H. Shapourian, A. Vishwanath, and M. A. Metlitski, Phys. Rev. B **104**, 104201 (2021).
[35] C. M. Duque, H.-Y. Hu, Y.-Z. You, V. Khemani, R. Verresen, and R. Vasseur, Phys. Rev. B **103**, L100207 (2021).
[36] N. G. Jones and R. Verresen, J. Stat. Phys. **175**, 1164 (2019).
[37] W. Ye, M. Guo, Y.-C. He, C. Wang, and L. Zou, SciPost Phys. **13**, 066 (2022).
[38] N. Tantivasadakarn, R. Thorngren, A. Vishwanath, and R. Verresen, SciPost Phys. **14**, 012 (2023).
[39] N. Tantivasadakarn, R. Thorngren, A. Vishwanath, and R. Verresen, SciPost Phys. **14**, 013 (2023).
[40] R. Thorngren, A. Vishwanath, and R. Verresen, Phys. Rev. B **104**, 075132 (2021).
[41] S.-C. Chang and P. Hosur, arXiv:2201.07260.
[42] R. Verresen, J. Bibo, and F. Pollmann, arXiv:2102.08967.
[43] S. Prembabu, R. Thorngren, and R. Verresen, Phys. Rev. B **109**, L201112 (2024).
[44] U. Borla, R. Verresen, J. Shah, and S. Moroz, SciPost Phys. **10**, 148 (2021).
[45] L. Li, M. Oshikawa, and Y. Zheng, Phys. Rev. B **108**, 214429 (2023).
[46] H. Yang, L. Li, K. Okunishi, and H. Katsura, Phys. Rev. B **107**, 125158 (2023).
[47] X. Wang, L. Li, and J. Wu, arXiv:2306.11446.
[48] S. Yang, Z. Pan, D.-C. Lu, and X.-J. Yu, Phys. Rev. B **108**, 245152 (2023).
[49] S. Mondal, A. Agarwala, T. Mishra, and A. Prakash, Phys. Rev. B **108**, 245135 (2023).
[50] Y. Hidaka, S. C. Furuya, A. Ueda, and Y. Tada, Phys. Rev. B **106**, 144436 (2022).
[51] R. Flores-Calderón, E. J. König, and A. M. Cook, arXiv:2311.17799.
[52] R.-Z. Huang, L. Zhang, A. M. Läuchli, J. Haegeman, F. Verstraete, and L. Vanderstraeten, Phys. Rev. Lett. **132**, 086503 (2024).
[53] S. Sachdev, *Quantum Phases of Matter* (Cambridge University Press, Cambridge, England, 2023).
[54] S. Sachdev, *Quantum Phase Transitions*, 2nd ed. (Cambridge University Press, Cambridge, England, 2011).
[55] J. Cardy, *Scaling and Renormalization in Statistical Physics* (Cambridge University Press, Cambridge, England, 1996), Vol. 5.
[56] P. Francesco, P. Mathieu, and D. Sénéchal, *Conformal field theory* (Springer Science & Business Media, New York, 2012).
[57] P. Ginsparg, arXiv:hep-th/9108028.
[58] L. Su and M. Zeng, Phys. Rev. B **109**, 245108 (2024).
[59] T. Ando, arXiv:2402.03566.
[60] X.-J. Yu, S. Yang, J.-B. Xu, and L. Xu, Phys. Rev. B **106**, 165124 (2022).
[61] P. Calabrese and J. Cardy, J. Stat. Mech. (2004) P06002.
[62] P. Calabrese and J. Cardy, J. Phys. A **42**, 504005 (2009).
[63] R. R. Kumar, N. Roy, Y. R. Kartik, S. Rahul, and S. Sarkar, Phys. Rev. B **107**, 205114 (2023).
[64] R. R. Kumar, Y. R. Kartik, and S. Sarkar, New J. Phys. **25**, 083027 (2023).
[65] R. Lundgren, J. Blair, P. Laurell, N. Regnault, G. A. Fiete, M. Greiter, and R. Thomale, Phys. Rev. B **94**, 081112(R) (2016).
[66] P. Calabrese and A. Lefevre, Phys. Rev. A **78**, 032329 (2008).
[67] F. Pollmann, A. M. Turner, E. Berg, and M. Oshikawa, Phys. Rev. B **81**, 064439 (2010).
[68] R. Thomale, D. P. Arovas, and B. A. Bernevig, Phys. Rev. Lett. **105**, 116805 (2010).
[69] X.-L. Qi, H. Katsura, and A. W. W. Ludwig, Phys. Rev. Lett. **108**, 196402 (2012).
[70] A. Chandran, V. Khemani, and S. L. Sondhi, Phys. Rev. Lett. **113**, 060501 (2014).
[71] R. Lundgren, J. Blair, M. Greiter, A. Läuchli, G. A. Fiete, and R. Thomale, Phys. Rev. Lett. **113**, 256404 (2014).
[72] D. Poilblanc, Phys. Rev. Lett. **105**, 077202 (2010).
[73] N. Laflorencie, Phys. Rep. **646**, 1 (2016).
[74] H. Yao and X.-L. Qi, Phys. Rev. Lett. **105**, 080501 (2010).
[75] L. Fidkowski, Phys. Rev. Lett. **104**, 130502 (2010).
[76] Y.-N. Zhou, X. Li, H. Zhai, C. Li, and Y. Gu, arXiv:2310.01475.
[77] C. Li, X. Li, and Y.-N. Zhou, Quantum Front. **3**, 9 (2024).
[78] A. M. Läuchli, arXiv:1303.0741.
[79] K. Ohmori and Y. Tachikawa, J. Stat. Mech. (2015) P04010.
[80] J. Cardy and E. Tonni, J. Stat. Mech. (2016) 123103.
[81] B. Swingle and T. Senthil, Phys. Rev. B **86**, 045117 (2012).
[82] Operator content in a 2D CFT means all operators present in the theory that form representations of the conformal symmetry. It generally includes primary fields and their descendants, reflecting the underlying structure of CFT. The scaling dimensions of these operators represent a unique structure of the underlying CFT or boundary CFT, which can be inferred, e.g., via the energy spectrum.
[83] J. L. Cardy, Nucl. Phys. **B240**, 514 (1984).
[84] J. L. Cardy, Nucl. Phys. **B275**, 200 (1986).
[85] J. L. Cardy, Nucl. Phys. **B324**, 581 (1989).
[86] R. Verresen, R. Moessner, and F. Pollmann, Phys. Rev. B **96**, 165124 (2017).
[87] Z.-X. Guo, X.-J. Yu, X.-D. Hu, and Z. Li, Phys. Rev. A **105**, 053311 (2022).
[88] T. H. Hsieh and L. Fu, Phys. Rev. Lett. **113**, 106801 (2014).
[89] A. M. Turner, F. Pollmann, and E. Berg, Phys. Rev. B **83**, 075102 (2011).

[90] N. G. Jones, J. Bibo, B. Jobst, F. Pollmann, A. Smith, and R. Verresen, Phys. Rev. Res. **3**, 033265 (2021).
[91] A. Smith, B. Jobst, A. G. Green, and F. Pollmann, Phys. Rev. Res. **4**, L022020 (2022).
[92] S. R. White, Phys. Rev. Lett. **69**, 2863 (1992).
[93] S. R. White, Phys. Rev. B **48**, 10345 (1993).
[94] U. Schollwöck, Rev. Mod. Phys. **77**, 259 (2005).
[95] U. Schollwöck, Ann. Phys. (Amsterdam) **326**, 96 (2011), January 2011 Special Issue.
[96] F. Verstraete and J. I. Cirac, Phys. Rev. B **73**, 094423 (2006).
[97] R. Orús, Ann. Phys. (Amsterdam) **349**, 117 (2014).
[98] E. Stoudenmire and S. R. White, Annu. Rev. Condens. Matter Phys. **3**, 111 (2012).
[99] See Supplemental Material at http://link.aps.org/supplemental/10.1103/PhysRevLett.133.026601 for details, which includes Refs. [100–105].
[100] R. Verresen, R. Thorngren, N. G. Jones, and F. Pollmann, Phys. Rev. X **11**, 041059 (2021).
[101] J. L. Cardy, Nucl. Phys. **B275**, 200 (1986).
[102] J. Cardy and E. Tonni, J. Stat. Mech. (2016) 123103.
[103] K. Ohmori and Y. Tachikawa, J. Stat. Mech. (2015) P04010.
[104] L. Li, M. Oshikawa, and Y. Zheng, arXiv:2204.03131.
[105] A. M. Läuchli, arXiv:1303.0741.
[106] M. Levin and Z.-C. Gu, Phys. Rev. B **86**, 115109 (2012).
[107] E. Witten, in *Dialogues Between Physics and Mathematics: CN Yang at 100* (Springer, New York, 2022), pp. 241–284.
[108] S. Eggert and I. Affleck, Phys. Rev. B **46**, 10866 (1992).
[109] J. J. Bisognano and E. H. Wichmann, J. Math. Phys. (N.Y.) **16**, 985 (1975).
[110] T. V. Zache, C. Kokail, B. Sundar, and P. Zoller, Quantum **6**, 702 (2022).
[111] C. Kokail, B. Sundar, T. V. Zache, A. Elben, B. Vermersch, M. Dalmonte, R. van Bijnen, and P. Zoller, Phys. Rev. Lett. **127**, 170501 (2021).
[112] M. K. Joshi, C. Kokail, R. van Bijnen, F. Kranzl, T. V. Zache, R. Blatt, C. F. Roos, and P. Zoller, Nature (London) **624**, 539 (2023).
[113] C. Kokail, R. van Bijnen, A. Elben, B. Vermersch, and P. Zoller, Nat. Phys. **17**, 936 (2021).
[114] W. J. L. Buyers, R. M. Morra, R. L. Armstrong, M. J. Hogan, P. Gerlach, and K. Hirakawa, Phys. Rev. Lett. **56**, 371 (1986).
[115] Y. Liu, Z. Wang, T. Sato, M. Hohenadler, C. Wang, W. Guo, and F. F. Assaad, Nat. Commun. **10**, 2658 (2019).
[116] N. Myerson-Jain, X.-C. Wu, and C. Xu, arXiv:2405.18481.
[117] T. Song, Y. Jia, G. Yu, Y. Tang, P. Wang, R. Singha, X. Gui, A. J. Uzan-Narovlansky, M. Onyszczak, K. Watanabe *et al.*, Nat. Phys. **20**, 269 (2024).
[118] X. Wan, A. M. Turner, A. Vishwanath, and S. Y. Savrasov, Phys. Rev. B **83**, 205101 (2011).
[119] B. Q. Lv, H. M. Weng, B. B. Fu, X. P. Wang, H. Miao, J. Ma, P. Richard, X. C. Huang, L. X. Zhao, G. F. Chen, Z. Fang, X. Dai, T. Qian, and H. Ding, Phys. Rev. X **5**, 031013 (2015).
[120] S.-Y. Xu, I. Belopolski, N. Alidoust, M. Neupane, G. Bian, C. Zhang, R. Sankar, G. Chang, Z. Yuan, C.-C. Lee *et al.*, Science **349**, 613 (2015).
[121] L. Lu, Z. Wang, D. Ye, L. Ran, L. Fu, J. D. Joannopoulos, and M. Soljačić, Science **349**, 622 (2015).
[122] M. Fishman, S. R. White, and E. M. Stoudenmire, SciPost Phys. Codebases **4** (2022).